Tunable continuous wave and femtosecond mode-locked Yb^{3+} laser operation in $NaLu(WO_4)_2$

A. García-Cortés, J. M. Cano-Torres, X. Han, C. Cascales, and C. Zaldo[a)]
Instituto de Ciencia de Materiales de Madrid, Consejo Superior de Investigaciones Científicas, c/ Sor Juana Inés de la Cruz 3, Cantoblanco, E-28049 Madrid, Spain

X. Mateos, S. Rivier, U. Griebner, and V. Petrov
Max-Born-Institute for Nonlinear Optics and Ultrafast Spectroscopy, 2A Max-Born-Strasse, D-12489 Berlin, Germany

F. J. Valle
Instituto de Cerámica y Vidrio, Consejo Superior de Investigaciones Científicas, c/ Kelsen 5, Cantoblanco, E-28049 Madrid, Spain

(Received 18 October 2006; accepted 15 December 2006; published online 27 March 2007)

Continuous wave and femtosecond mode-locked laser operation of Yb^{3+} in the tetragonal $NaLu(WO_4)_2$ crystal host is demonstrated by pumping with a Ti:sapphire laser. Pumping with 1.8 W at 974 nm, a maximum output power of 650 mW was achieved at 1029.6 nm. The slope efficiency was in excess of 60%. The laser performance was similar for the two polarizations. By inserting a birefringent filter the output wavelength was tunable from 1010 to 1055 nm. Pulses as short as 90 fs with an average power of 50 mW were generated by passive mode locking at a repetition rate of 95 MHz. These attractive laser properties of $NaLu_{1-x}Yb_x(WO_4)_2$ are related to the inhomogeneous broadening of the Yb^{3+} spectral features resulting from the local disorder of the host crystal. We report the spectroscopic properties of Yb^{3+} in the 5–300 K temperature range and the optical properties of the host at room temperature. © *2007 American Institute of Physics*.
[DOI: 10.1063/1.2490382]

I. INTRODUCTION

Yb^{3+}-based lasers are an attractive alternative to Nd^{3+} lasers for the 1 μm spectral range due to the higher efficiency that can be obtained by pumping with the more robust InGaAs laser diodes near 980 nm in comparison with the use of AlGaAs diodes emitting near 800 nm. This is related to the smaller quantum defect of Yb. As a consequence the thermal load to the crystal is also reduced. Moreover, the simpler energy level structure of Yb avoids optical losses by upconversion and by other nonlinear excitation mechanisms. To produce femtosecond laser pulses, a broad emission linewidth is required. Due to the stronger electron-phonon coupling the linewidths of Yb, both absorption and emission, are broader than those of Nd. Additional broadening can be expected in materials with structural disorder. The tetragonal (space group $I\bar{4}$, N° 82) double tungstate (DT) and double molybdate (DM) crystals with general formula $M^+T^{3+}(XO_4)_2$ (X=W or Mo) are locally disordered materials, promising as rare-earth laser hosts for applications requiring tunability or ultrashort pulses. Yb laser operation has been demonstrated in several such crystal hosts grown by the Czochralski (Cz) method: $NaT(WO_4)_2$, T=La (Ref. 1) or Gd (Refs. 2 and 3) and $NaT(MoO_4)_2$, T=La.[1,4,5] The laser performance critically depends on the crystal optical quality and Yb concentration. Yb-doped $NaGd(WO_4)_2$ (hereafter $NaGd/Yb_xW$) has outstanding laser properties: 16.5 W of cw laser power have been obtained with diode pumping in a thin disk cavity geometry,[6] and 65 nm of laser tunability around 1050 nm have been achieved along with 120 fs short laser pulses.[3] However, the $NaT_{1-x}Yb_x(WO_4)_2$ compounds with $x_{melt}>0.2$ have incongruent melting character and therefore the Yb incorporation in Cz-grown crystals is limited to about $x=0.15$. Hence, further efforts are necessary to synthesize tetragonal DT and DM crystals with higher Yb concentration by using other crystal growth methods.

For the typical peak absorption and emission cross sections of Yb in disordered DT and DM crystals, $\approx 1\ldots.2\times10^{-20}$ cm^2, Yb concentrations exceeding 20 mol % are necessary for the preparation of thin (<0.2 mm) active elements to be implemented in a thin disk cavity geometry. Since such elements are fragile and inconvenient for handling, as an alternative, layers with thickness below 0.2 mm can be grown on transparent substrates by liquid phase epitaxy (LPE). In the latter case the composition of the laser active Yb-doped layer must be selected, taking into account the substrate properties. From this point of view the combination of active $NaLu_{1-x}Yb_x(WO_4)_2$ ($NaLu/Yb_xW$) layers with passive (transparent) $NaLu(WO_4)_2$ (NaLuW) substrates will ensure less stress and interfacial defect density due to the close ionic radii of Yb and Lu as well as the close crystal lattice parameters of $NaYb(WO_4)_2$ and NaLuW which are isostructural crystals.

In this work we report the growth of $NaLu/Yb_xW$ crystals with up to $x_{melt}=0.5$ Yb content, determine the basic optical properties of the NaLuW host and the spectroscopic

[a)]Author to whom correspondence should be addressed; electronic mail: cezaldo@icmm.csic.es

TABLE I. Growth conditions and composition of $NaLu_{1-x}Yb_x(WO_4)_2$ crystals grown by the TSSG method.

x_{melt}	Solute/flux molar ratio	Cooling interval (K)	Cooling rate (K/h)	Crystal formula	Yb density (10^{21} cm^{-3})
0.005	1:4	1150–1118	0.03	$Na_{1.011}Lu_{0.997}Yb_{0.006}W_{0.998}$	0.038
0.1	1:6	1107–1097	0.02	$Na_{1.027}Lu_{0.874}Yb_{0.111}W_{1.001}$	0.746
0.5	1:3.5	1190–1176	0.04	$Na_{1.014}Lu_{0.481}Yb_{0.508}W_{1.001}$	3.40

properties of Yb^{3+}, and demonstrate tunable cw and mode-locked laser operation with $NaLu/Yb_xW$, $x_{melt}=0.1$.

II. CRYSTAL GROWTH AND HOST CHARACTERIZATION

We used a $Na_2W_2O_7$ flux and the top seeded solution growth (TSSG) method to prepare $NaLu/Yb_xW$ crystals. The initial products from Johnson Matthey were 99.5% Na_2CO_3, 99.8% W_2O_3, 99.99% Lu_2O_3, and 99.9% Yb_2O_3. Three Yb doping levels were used with different purposes: $x_{melt}=0.005$ for spectroscopic analysis, $x_{melt}=0.1$ for laser studies at a doping level comparative to previous works on isostructural crystals, and finally $x_{melt}=0.5$ to explore the incorporation of high Yb concentrations. The initial products were mixed in the required solute (crystal)/flux compositions. The solute/flux mixtures were melted in Pt crucibles and held for several days at ≈50 K above the melting temperature for homogenization. As seeds, Pt wire and *c*-cut NaGdW crystals were used. The seed rotation was at 10–30 rpm. Table I summarizes the growth conditions for the three crystals. The crystal composition was determined by x-ray fluorescence spectrometry (XRFS) using specially developed $NaLu/Yb_xW$ standards melted with $Li_2B_4O_7$.

The optical properties of the NaLuW host were studied at room temperature using samples with the lowest Yb concentration. The optical absorption was measured with a Varian (model Cary 5E, λ=200–3000 nm) and a Bruker (model IFS66v/S, λ=1.3–200 μm) spectrophotometers. Figure 1 shows the transparency range of NaLuW. The ultraviolet (UV) absorption edge (cutoff wavelength) obtained by linear extrapolation is slightly shorter for the σ polarization. It is worth noting that NaLuW has the largest band gap among the tetragonal DT and DM crystals so far studied, see Fig. 1. The transparency extends in the infrared up to the onset of two-phonon absorption near 4 μm related to $(WO_4)^{2-}$ vibrations.

The ordinary n_o ($\perp$c) and extraordinary n_e ($\|c$) refractive indices of NaLuW were measured at room temperature by the minimum deviation method using prisms. Figure 2 shows the results and the fit to the single-pole Sellmeier law $n^2=A+\{B/[1-(C/\lambda)^2]\}-D\lambda^2$ with the values of the four parameters given in the figure inset. It is interesting to note that NaLuW has larger refractive index in comparison with other related transparent hosts, Na*T*W, *T*=La (Ref. 7) or Gd,[3] with the exception of *T*=Bi.[8]

The Raman spectra of NaLuW have not been reported in the literature yet. Figure 3 shows the spontaneous Raman spectra recorded at 300 K under polarized conditions using a Jobin-Yvon HR 460 monochromator and a N_2 cooled charge coupled device. A backscattering geometry was employed, with configurations $b(cc)\bar{b}$, $b(aa)\bar{b}$, and $b(ca)\bar{b}$, labeled according to the usual Porto notation. The samples were excited with the 514.5 nm line of an Ar–Kr laser (Spectra-Physics). The incident beam was focused on the sample surface using an Olympus microscope with an objective of small numerical aperture and the scattered light was collected with the same optical system using a Kaiser Supernotch filter to eliminate the elastically scattered light. The Raman shift was calibrated by using the 520 cm^{-1} phonon of a single crystal of Si as a reference. The Raman scattered light is strongly polarized, parallel to the excitation light. The

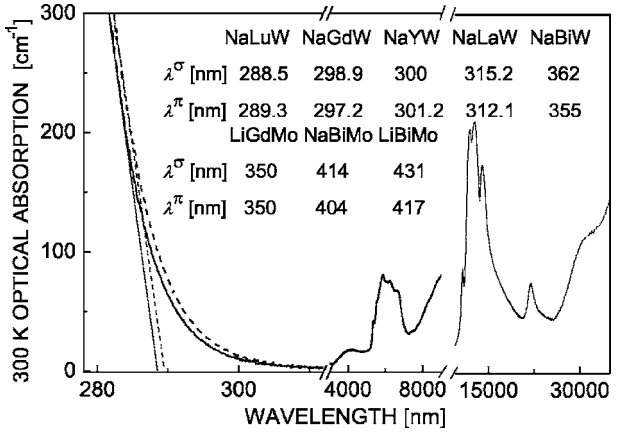

FIG. 1. Optical absorption of $NaLu(WO_4)_2$ measured at 300 K. Polarized spectra in the ultraviolet limit: σ, solid curve and π, dashed curve. The extrapolated straight lines are used to determine the ultraviolet UV edges. The infrared spectra are unpolarized and the absorption scale is arbitrary above 10 000 nm. In the abbreviated formulas W means $(WO_4)_2$ and Mo means $(MoO_4)_2$.

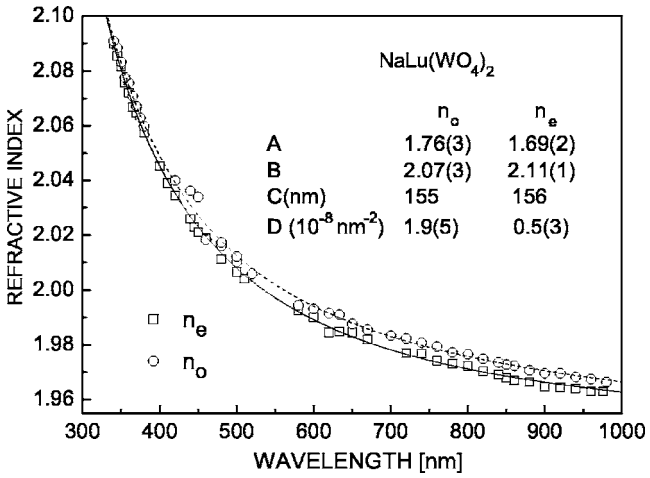

FIG. 2. Ordinary n_o and extraordinary n_e refractive indices of $NaLu(WO_4)_2$ measured at 300 K. The symbols are the experimental points and the curves are the fits to the Sellmeier law with parameters summarized in the inset.

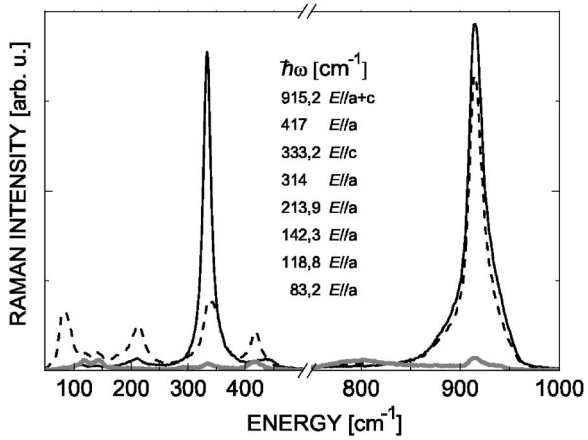

FIG. 3. Polarized Raman spectra of $NaLu(WO_4)_2$. $b(cc)\bar{b}$ (solid line), $b(aa)\bar{b}$ (dashed line), and $b(ca)\bar{b}$ (gray line). For a tetragonal crystal the a and b axes are equivalent.

most intense peak at 915 cm^{-1} with a full width at half maximum (FWHM) of $\Delta\Omega_R \approx 16$ cm^{-1} is observed either for light polarized parallel to the crystal a axis, $E\|a$ or the c axis, $E\|c$. It exhibits a shoulder at 921 cm^{-1}. Another intense Raman line is observed for $E\|c$ at 333 cm^{-1} (FWHM $=17$ cm^{-1}). The phonon energies of the other Raman peaks are included in Fig. 3. The large $\Delta\Omega_R$ values correspond to short dephasing times, $T_R=[\pi c\Delta\Omega_R]^{-1}\approx 0.6$ ps. This suggests that NaLuW can be pumped in the picosecond regime to shift the laser wavelength by stimulated Raman scattering.[9]

III. Yb^{3+} SPECTROSCOPY

It has been recently shown that some tetragonal DT and DM crystals have the symmetry of space group $I\bar{4}$ (N° 82)[3,10] therefore two nonequivalent 2*b* and 2*d* lattice sites are shared by *M* and *T* ions with specific occupancy factors. Yb^{3+}, replacing Lu in $NaLu/Yb_xW$, is also expected to occupy both sites, each of them with several different environments due to the near-to-random distribution of Na and Lu ions in the first cationic neighbor shell. The spectral contributions of these two Yb sites were investigated by 5 K optical spectroscopy. The spectroscopic results were also used to derive the Yb^{3+} energy levels. Figure 4(a) shows the polarized 5 K optical absorption of $NaLu/Yb_xW$. The different bands correspond to $^2F_{7/2}(n=0)\rightarrow{}^2F_{5/2}(n'=0',1',2')$ electronic transitions. The overlapping bands observed in the σ spectrum between 920 and 950 nm are ascribed to $0\rightarrow 2'$ transitions, those observed in the σ and π spectra between 950 and 970 nm are ascribed to $0\rightarrow 1'$ transitions, and finally the apparently single band centered at 973.3 nm in the σ and π spectra is ascribed to the $0\rightarrow 0'$ transitions. Therefore, the σ spectrum shows all Yb^{3+} transitions.

Figure 5 shows the σ-polarized 5 K photoluminescence. The emission spectrum exhibits four main bands associated with the $^2F_{5/2}(n'=0')\rightarrow{}^2F_{7/2}(n=0,1,2,3)$ transitions, but the line shape and the spectral positions of the peaks depend on the excitation wavelength. The emission changes are most clearly observed for the band near 995 nm. The excitation spectra (formally equivalent to the optical absorption ones)

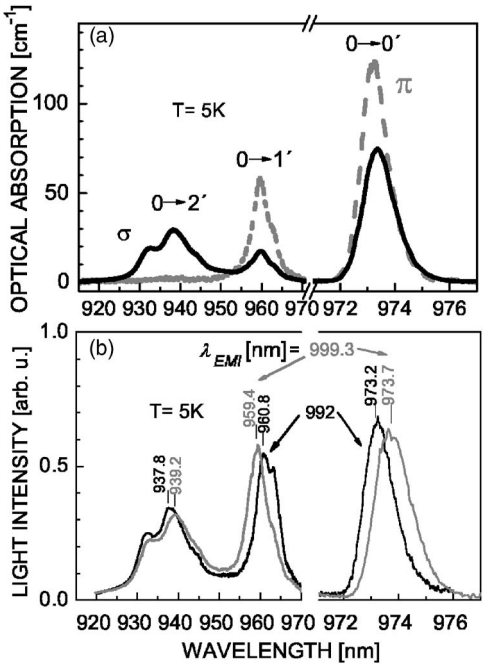

FIG. 4. 5 K polarized optical absorption spectra of $NaLu/Yb_xW$ ($x_{melt}=0.1$) (a) and 5 K excitation spectra of $NaLu/Yb_xW$ ($x_{melt}=0.005$) (b).

in turn depend on the detected wavelength and allow to reveal the Yb site contributions. Figure 4(b) shows the excitation spectra corresponding to the high and low energy arms of the $0'\rightarrow 1$ emission band near 995 nm. The composite band related to the $0\rightarrow 0'$ transition contains contributions from two overlapping bands with peaks at 973.7 and 973.2 nm. We ascribe these two bands to contributions of Yb^{3+} in the 2*b* and 2*d* sites. The two contributions can be observed in the $0\rightarrow 1'$ band in the excitation spectrum at 960.8 and 959.4 nm, with a secondary band at 963.2 nm seen as a shoulder. Finally, in the 920–950 nm spectral range corresponding to the $0\rightarrow 2'$ transition, three overlapping bands are present independent of the emission wavelength. The individual contribution of Yb^{3+} in the two sites is responsible for the different positions, 937.8 and 939.2 nm, of the central peak. Both sets of Stark energy levels determined from the above experiments are summarized in Table II.

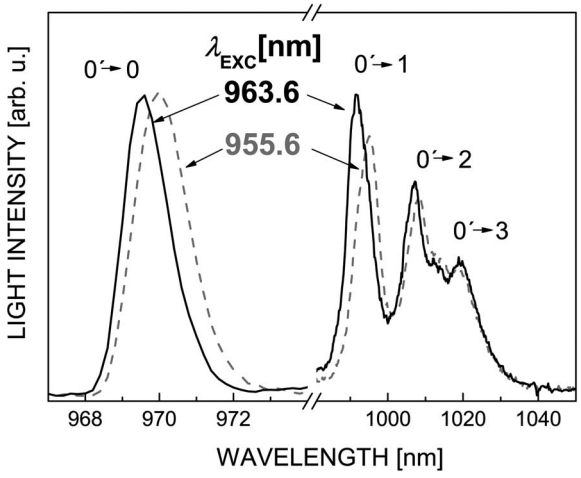

FIG. 5. 5 K photoluminescence spectrum of $NaLu/Yb_xW$ ($x_{melt}=0.005$).

TABLE II. FI (E^0 and ζ) parameters and calculated SOM CFPs (B_0^2, B_0^4, B_4^4, B_0^6, B_4^6, and S_4^6) used to calculate the $^2F_{7/2}(n)$ and $^2F_{5/2}(n')$ energy levels of Yb^{3+} in the 2*b* and 2*d* sites of NaLuW. The experimentally determined Yb energy levels are given in parentheses. All energies are relative to the $^2F_{7/2}(0)$ level for the corresponding site. Parameters and energies are given in cm^{-1}. Overlap between Yb-ligand (oxygen) orbital wave functions: $\rho=0.07$, effective charge for oxygen: −1.

Site	2*d*	2*b*
E^0	4642.15	
ζ	2900.00	2902.00
B_0^2	402	485
B_0^4	−734	−727
B_4^4	±745	±718
B_0^6	−23	2
B_4^6	±651	±639
S_4^6	±110	±101
$^2F_{5/2}(2')$	10 645 (10 647)	10 665 (10 663)
$^2F_{5/2}(1')$	10 420 (10 423)	10 404 (10 408)
$^2F_{5/2}(0')$	10 270 (10 270)	10 276 (10 275)
$^2F_{7/2}(3)$	496 (474)	518 (475)
$^2F_{7/2}(2)$	383 (378)	370 (372)
$^2F_{7/2}(1)$	280 (239)	255 (238)
$^2F_{7/2}(0)$	0 (0)	0 (0)

In order to assess the above interpretation of the 5 K excitation spectra, the obtained energy level sets were compared with those computed using the semiempirical simple overlap crystal field model (SOM),[11] which allows to estimate the crystal field parameters (CFPs) from the crystallographic positions of the Lu (or Yb) O_8 coordination polyhedra. Separate sets of CFPs for the Yb^{3+} ions in the 2*b* and 2*d* sites were derived from the atomic coordinates and the corresponding Yb–O bond distances obtained from a comprehensive crystallographic study which will be published elsewhere. The calculated values of the six CFPs corresponding to the S_4 symmetry were then used, independently for each site, in the simulation of the $^2F_{7/2}(n)$ and $^2F_{5/2}(n')$ Stark level energies for the $4f^{13}$ configuration. The simulation was performed using a previously developed code.[12] The used free ion (FI) parameters, the derived SOM CFPs, and the corresponding energy level schemes obtained for Yb^{3+} in each of the two sites are also included in Table II.

The comparison in Table II allows to assign the individual contributions of the 2*b* and 2*d* Yb^{3+} sites in the 5 K spectra shown in Fig. 4. In particular, the sequence for the $^2F_{5/2}$ $(0',1',2')$ energy levels experimentally obtained by selective excitation is very well reproduced by the simulation. Moreover, the additional band structure observed in the 920–950 nm range should be related to other interactions, since the crystal field changes cannot account for such large energy level differences.

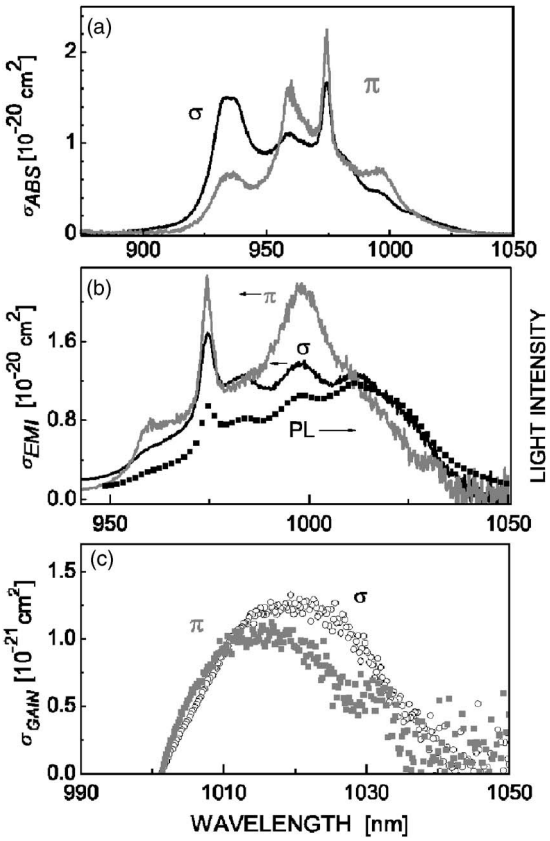

FIG. 6. 300 K cross sections of NaLu/Yb_xW. Absorption cross sections (σ_{abs}) (a). Emission cross sections (σ_{emi}) (b). The 300 K σ-polarized photoluminescence (PL) recorded with $\lambda_{exc}=939$ nm is included for comparison (squares). Gain cross sections (σ_{gain}) for $\beta=0.2$ (c).

The absorption cross sections σ_{abs} were calculated from absorption measurements performed at room temperature with a NaLu/Yb_xW ($x_{melt}=0.5$) sample in order to minimize the errors from the determination of the exact Yb concentration and to have more reliable optical absorption data in the long-wave wing, necessary for accurate computation of the emission cross sections. Table III shows a comparison of the peak σ_{abs} of Yb^{3+} in NaLuW and other isostructural DT crystal hosts. It can be seen that the largest σ_{abs} so far found corresponds to the NaLuW host. It is likely that this is related to the stronger crystal field induced by the smaller lattice volume of NaLuW.

The emission cross sections can be obtained for both polarizations using the reciprocity method[13] as $\sigma_{emi}=\sigma_{abs}(Z_l/Z_u)e^{(E_{zl}-h\nu)/k_BT}$, where for NaLu/$Yb_xW$ crystals $Z_l/Z_u=0.957$ and $E_{zl}=10\,273$ cm^{-1} are calculated using the average of the 2*d* and 2*b* energy levels given in Table II. Figure 6(b) shows a comparison of the calculated σ_{emi} and the measured photoluminescence at 300 K. The difference observed at short wavelengths is due to reabsorption.

The $^2F_{5/2}$ Yb^{3+} fluorescence lifetime was measured by

TABLE III. Absorption (σ_{abs}) and emission (σ_{emi}) cross sections of Yb^{3+} in tetragonal double tungstates.

	Cz NaLaW	Cz NaGdW	TSSG NaLuW
σ_{abs} (σ/π) (10^{-20} cm^2), λ (nm)	1.15/1.60, 976	1.36/1.78, 975	1.65/2.22, 973.8
σ_{emi} (σ/π) (10^{-20} cm^2), λ (nm)	0.94/2.28, 1000	0.75/1.89, 1000	1.4/2.1, 1000

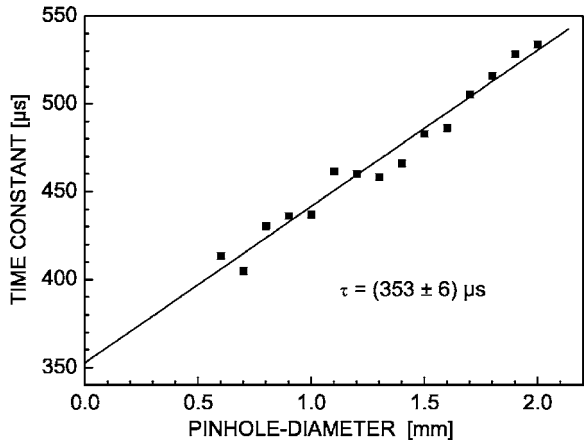

FIG. 7. $^2F_{5/2}$ Yb^{3+} fluorescence lifetime obtained by extrapolation to zero pinhole diameter of the decay time constants measured at room temperature.

the pinhole method[14] to avoid radiation trapping effects. The result obtained at 300 K with a $NaLu/Yb_{0.1}W$ sample is $\tau = 353 \pm 6$ μs (Fig. 7). The radiative lifetime can be obtained by the Füchtbauer-Ladenburg method,

$$\tau_{\mathrm{rad}} = \frac{1}{8\pi n^2 c}\left[\int \frac{\langle \sigma_{\mathrm{emi}}(\lambda)\rangle}{\lambda^4} d\lambda\right]^{-1},$$

where the average is over the polarization. Taking into account the refractive index data in Fig. 2, i.e., assuming an average value of $n \approx 1.966$, one arrives at $\tau_{\mathrm{rad}} = 368$ μs. This gives an intrinsic quantum efficiency of 0.96.

The expected oscillation wavelength can be predicted calculating the gain cross section $\sigma_{\mathrm{gain}}(\lambda) = \beta\sigma_{\mathrm{emi}}(\lambda) - (1-\beta)\sigma_{\mathrm{abs}}(\lambda)$, where β is the inversion ratio. Figure 6(c) shows the calculated gain cross sections for $\beta = 0.2$ in the σ and π polarization configurations. From these curves, it can be expected that, for constant cavity losses, the oscillation wavelength will be somewhat shorter for the π polarization.

IV. LASER OPERATION

Continuous wave (cw) laser operation of $NaLu/Yb_xW$ ($x_{\mathrm{melt}} = 0.1$) was studied in the astigmatically compensated Z-shaped cavity shown in Fig. 8(a). The two folding mirrors M2 and M3 had a radius of curvature (RC) of −10 cm. The cavity length was ~140 cm. The 1.16 and 0.94 mm thick $NaLu/Yb_{0.1}W$ samples used were uncoated and placed under Brewster angle between the two folding mirrors. No special cooling was applied. The *a*-cut 1.16 mm thick sample allowed to study both σ and π polarizations in this laser, and the pump polarization applied was always in the same plane. The cut of the 0.94 mm thick sample allowed to study only the σ polarization. The $NaLu/Yb_xW$ samples were pumped with a Ti:sapphire laser (linewidth ≈1 nm) at 974 nm using a 6.28 cm focusing lens (FL) [Fig. 8(a)]. The crystal absorption was estimated under lasing conditions and also with lasing interrupted.

Figure 9 shows the change of the crystal absorption (single-pass pumping) measured with increasing incident pump power. In the absence of lasing, strong absorption bleaching is observed. In this case the measured absorption does not depend on the output coupler used and the scatter in the data is representative of the accuracy of the measurement. Laser operation had a recycling effect: the intracavity intensity increases the pump saturation intensity and the bleaching effect is suppressed. As a consequence, the actual crystal absorption is weakly dependent on the incident pump power. The behavior of the absorption was similar for the two polarizations; the absorption was only slightly higher for the π polarization.

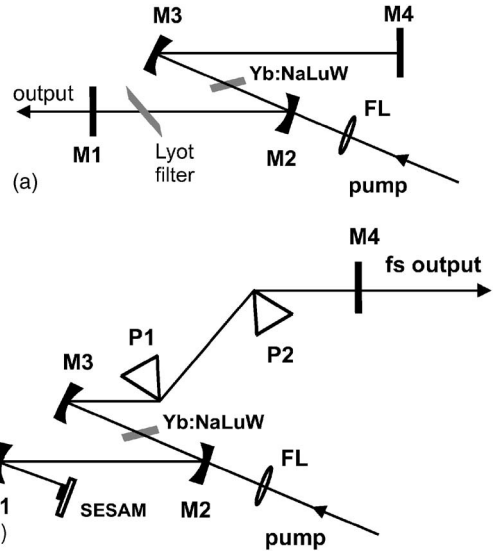

FIG. 8. Cavity configurations used in the cw (a) and mode-locked (b) regimes of the $NaLu/Yb_{0.1}W$ laser.

The cw laser operation results obtained with the 1.16 mm thick sample are summarized in Fig. 10. Up to the maximum pump power applied, which corresponded to absorbed powers exceeding 1 W, the output power was linearly proportional to the absorbed power, i.e., no thermal effects were observed. The maximum output power of 463 mW was obtained with a $T_{\mathrm{OC}} = 3\%$ output coupler for π polarization at an absorbed pump power of 1.14 W. The maximum slope efficiency with respect to the absorbed power was obtained for π polarization and $T_{\mathrm{OC}} = 5\%$ and $\eta = 60.9\%$. The oscilla-

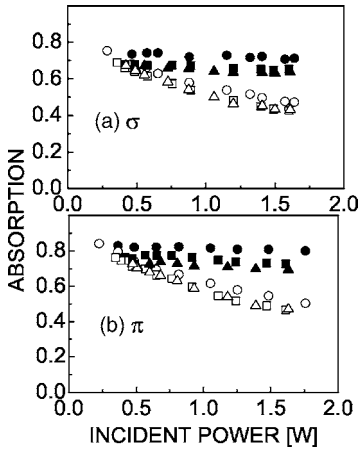

FIG. 9. Single-pass absorption of the 1.16 mm thick $NaLu/Yb_{0.1}W$ vs incident pump power measured without lasing (open symbols) and under laser operation (filled symbols) for σ polarization (a) and π polarization (b) and several output coupler transmissions T_{OC}: 1% (circles), 3% (squares), and 5% (triangles).

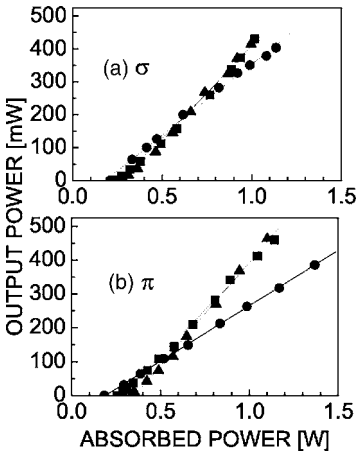

FIG. 10. Output power vs absorbed pump power at 974 nm of the cw $NaLu/Yb_{0.1}W$ laser for σ (a) and π (b) polarizations using several output coupler transmissions T_{OC}: 1% (circles), 3% (squares), and 5% (triangles). The linear fits shown give the slope efficiencies obtained for each T_{OC} value.

tion wavelength λ_L slightly decreased with T_{OC}, from 1036.9 nm ($T_{OC}=1\%$) to 1026.8 nm ($T_{OC}=5\%$) for the π polarization. For the σ polarization, the oscillation wavelengths were slightly longer, decreasing from 1041 nm ($T_{OC}=1\%$) to 1028.6 nm ($T_{OC}=5\%$), in agreement with the predictions of Fig. 6(c).

Higher output powers were obtained by recycling roughly 80% of the residual pump in a double-pass configuration. In this case M3 and M4 [Fig. 8(a)] were substituted by mirrors reflecting also the pump radiation and we used a Faraday isolator to avoid any feedback to the Ti:sapphire pump laser. With this setup it was difficult to measure accurately the double-pass absorption under lasing conditions but the single-pass absorption of the 0.94 mm thick crystal used was lower: 55%–60% under lasing conditions, depending on the output coupler. Therefore Fig. 11 shows the output laser power versus the incident pump power obtained with this sample for σ polarization. A maximum output power of 650 mW was achieved for an incident pump power of 1.8 W with $T_{OC}=3\%$; the maximum output with $T_{OC}=5\%$ was similar, 647 mW.

The cw laser tunability was studied with an intracavity two-plate birefringent filter in the cavity arm containing the

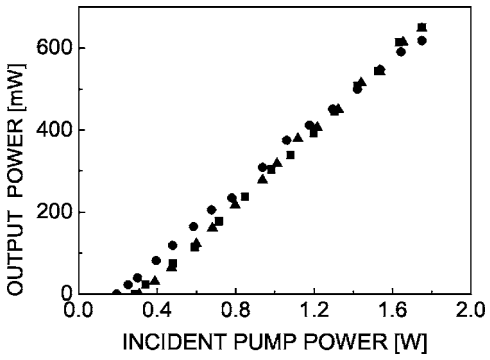

FIG. 11. Output power vs incident pump power at 974 nm for the cw $NaLu/Yb_{0.1}W$ laser using a double-pass pump configuration with the 0.94 mm thick sample and several output couplers, $T_{OC}=1\%$ (circles), 3% (squares), and 5% (triangles).

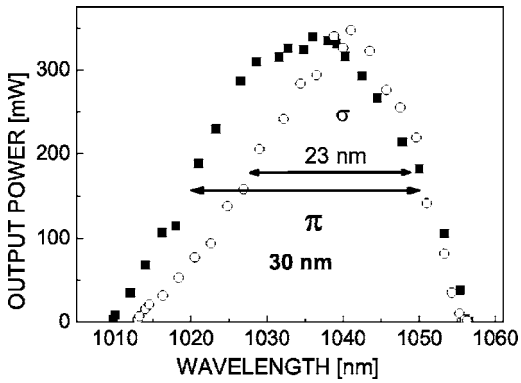

FIG. 12. Wavelength tunability under single-pass Ti:sapphire laser pumping of the 1.16 mm thick $NaLu/Yb_{0.1}W$ sample for $T_{OC}=1\%$ and the two polarizations.

output coupler (M1-M2), see Fig. 8(a). Figure 12 shows the results obtained with the 1.16 mm thick $NaLu/Yb_xW$ sample for the two polarizations. The incident pump power was 1.6 W. Continuous tuning was achieved from 1010 to 1055 nm for the π polarization; the FWHM of the tuning curve is 30 nm. For the σ polarization the tuning range was only slightly narrower as could be expected from the small difference in the gain cross sections, see Fig. 6(c). The experimental tuning ranges are limited on the short wavelength side by the reflectivity of the pump incoupling mirror M2 [Fig. 8(a)]. The achieved tuning ranges compare well with the results reported with Yb:NaGdW (Ref. 2) and Yb:NaLaW (Ref. 1) crystals of similar optical quality. Broader tuning has been demonstrated only with Yb-:NaGdW; however, these samples had superior optical quality.[3] Hence, improvement of the present tuning results can also be expected once the TSSG process for $NaLu/Yb_xW$ is optimized.

The mode-locking experiments were performed for the more promising π polarization with the same 1.16 mm thick sample used in the cw laser studies. The incident pump power was 1.45 W. The extended cavity configuration used is shown in Fig. 8(b). It included two SF10 prisms with a tip-to-tip separation of 32 cm inserted into the arm containing the output coupler and an additional RC=−10 cm mirror in the other arm to increase the fluence on the semiconductor saturable absorber mirror (SESAM) which terminated the resonator. The total cavity length corresponded to a repetition frequency of 95 MHz. The SESAM used for mode locking (a 10 nm thick single InGaAs quantum well implanted with As ions and embedded in a GaAs layer) was grown by metal organic vapor phase epitaxy. It was reflecting from 1000 to 1080 nm, the saturable absorption amounted to ~1%, and the relaxation time was 5 ps.

Using an output coupler with $T_{OC}=1\%$ and depending on the alignment it was possible to obtain pulses as short as 90 fs (FWHM assuming a $sech^2$-pulse shape) at an average output power of 50 mW or longer pulses (170 fs) for an average power of 130 mW. In both cases the spectrum was centered at 1040 nm. The intensity autocorrelation trace with the corresponding fit and the spectrum of the shortest pulses are shown in Fig. 13. The resulting time-bandwidth product

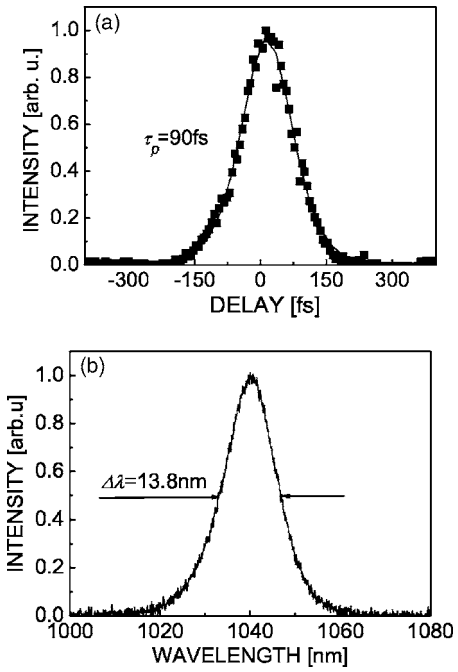

FIG. 13. Autocorrelation trace with the corresponding fit assuming $sech^2$-pulse shape (a) and spectrum (b) of the femtosecond $NaLu/Yb_{0.1}W$ laser with $T_{OC}=1\%$.

is 0.344, which is only slightly above the Fourier limit for a $sech^2$ pulse (0.315). No tendencies for Q-switching instabilities were observed.

V. CONCLUSIONS

We have demonstrated that 50% substitution of Lu by Yb is possible in tetragonal disordered crystals of $NaLu/Yb_xW$ grown by the TSSG technique. The contributions of Yb ions in two nonequivalent lattice sites explain the specific spectroscopic features observed at 5 K. The Yb^{3+} absorption and emission bands are characterized by inhomogeneous broadening related to the random occupancy of these two sites by Na^+ and T^{3+} (Lu and Yb) ions. These broad bands make the $NaLu/Yb_xW$ crystal attractive for tunable and mode-locked laser operation in the 1 μm spectral range. Output powers as high as 650 mW were achieved in the cw laser regime with Ti:sapphire laser pumping. The $NaLu/Yb_xW$ laser was continuously tunable over 45 nm. Realization of passive mode locking using a SESAM yielded bandwidth-limited pulses as short as 90 fs.

ACKNOWLEDGMENTS

This work was supported by Projects Nos. NMP3-CT-2003-505580 (EU), MAT2004-21113E, and MAT2005-6354-C03-01 (Spain). The experimental contributions of A. de Andrés in Raman (ICMM-CSIC) and of C. Kränkel and K. Petermann (Hamburg University) in lifetime measurements are also acknowledged. A.G. (FPU2003-018), X.H. (JC12006-4015-2459) and X.M. (EX2004-1294) are supported by grants from the Spanish government. X.M. additionally acknowledges support from the European Science Foundation.

[1] J. Liu *et al.*, Phys. Status Solidi A **202**, R29 (2005).
[2] M. Rico, J. Liu, U. Griebner, V. Petrov, M. D. Serrano, F. Esteban-Betegón, C. Cascales, and C. Zaldo, Opt. Express **12**, 5362 (2004).
[3] C. Cascales *et al.*, Phys. Rev. B **74**, 174114 (2006).
[4] M. Rico, J. Liu, J. M. Cano-Torres, A. García-Cortés, C. Cascales, C. Zaldo, U. Griebner, and V. Petrov, Appl. Phys. B: Lasers Opt. **81**, 621 (2005).
[5] A. V. Mandrik, A. E. Troshin, V. E. Kisel, A. S. Yasukevich, G. N. Klavsut, N. V. Kuleshov, and A. A. Pavlyuk, Appl. Phys. B: Lasers Opt. **81**, 1119 (2005).
[6] R. Peters, C. Kränkel, K. Petermann, and G. Huber, Adv. Solid-State Photonics, Vancouver (BC), Canada, Jan. 28–31, 2007, Conference Program and Technical Digest, OSA (Washington, DC), paper MA4.
[7] J. Liu *et al.*, Opt. Laser Technol. **39**, 558 (2007).
[8] V. Volkov, M. Rico, A. Méndez-Blas, and C. Zaldo, J. Phys. Chem. Solids **63**, 95 (2002).
[9] T. T. Basiev, A. A. Sobol, P. G. Zverev, V. V. Osiko, and R. C. Powell, Appl. Opt. **38**, 594 (1999).
[10] M. Rico, A. Méndez-Blas, V. Volkov, M. A. Monge, C. Cascales, C. Zaldo, A. Kling, and M. T. Fernández-Díaz, J. Opt. Soc. Am. B **23**, 2066 (2006).
[11] P. Porcher, M. Couto dos Santos, and O. Malta, Phys. Chem. Chem. Phys. **1**, 397 (1999).
[12] A. Méndez-Blas, M. Rico, V. Volkov, C. Cascales, C. Zaldo, C. Coya, A. Kling, and L. C. Alves, J. Phys.: Condens. Matter **16**, 2139 (2004).
[13] D. E. McCumber, Phys. Rev. **136**, A954 (1964).
[14] K. Petermann *et al.*, J. Cryst. Growth **275**, 135 (2005).